RESTRICTED INVESTIGATION REPORT 1754R

CSIRO

INSTITUTE OF MINERALS, ENERGY AND CONSTRUCTION

DIVISION OF EXPLORATION GEOSCIENCE

MAGNETIC PROPERTIES OF MAGNETITE-BEARING PYRITIC SCHISTS FROM THE RUDALL METAMORPHIC COMPLEX AND MODELLING OF THE ASSOCIATED MAGNETIC ANOMALY

D.A. CLARK

P.O. Box 136
North Ryde, NSW
Australia 2113

MAY, 1988

CSIRO

Division of Mineral Physics and Mineralogy
Delhi Road, North Ryde, NSW, Australia

A Division of the Institute of Energy and Earth Resources

CHIEF
Dr B. J. J. Embleton

PO Box 136, North Ryde, NSW, Australia 2113
Telephone (02) 887 8666
Telex AA25817
Facsimile (02) 887 8909

POLICY ON RESTRICTED INVESTIGATION REPORTS

Restricted Investigation Reports issued by this Division deal with projects where CSIRO has been granted privileged access to research material. In return for this access, they provide recipients with an opportunity to take advantage of results obtained on their samples or problems. Initially, circulation of Restricted Investigation Reports is strictly controlled, and we treat them as confidential documents at this stage. They should not be quoted publicly, but may be referred to as a "personal communication" from the author(s) if my approval is sought and given beforehand.

The results embodied in a Restricted Investigation Report may eventually form part of a more widely circulated CSIRO publication. Agreements with sponsors or companies generally specify that drafts will be first submitted for their approval, to ensure that proprietary information of a confidential nature is not inadvertently included.

After a certain period of time, the confidentiality of particular Restricted Investigation Reports will no longer be an important issue. It may then be appropriate for CSIRO to announce the titles of such reports, and to allow inspection and copying by other persons. This procedure would disseminate information about CSIRO research more widely to Industry. However, it will not be applicable to all Restricted Investigation Reports. Proprietary interests of various kinds may require an extended period of confidentiality. Premature release of Restricted Investigation Reports arising from continuing collaborative projects (especially AMIRA projects) may also be undesirable, and a separate policy exists in such cases.

You are invited to express an opinion about the security status of the enclosed Restricted Investigation Report. Unless I hear to the contrary, I will assume that in eighteen months time I have your permission to place this Restricted Investigation Report on open file, when it will be generally available to interested persons for reading, making notes, or photocopying, as desired.

APRIL 1987

B.J.J. Embleton
CHIEF OF DIVISION

DISTRIBUTION LIST

	Copy No.
CRAE (Belmont)	1-2
R. Smith	3
CSIRO Division of Exploration Geoscience	
D.A. Clark	4
P.W. Schmidt	5
B.J.J. Embleton	6
CSIRO IMEC Records	7

This is copy number 5 of 7

CONTENTS

LIST OF TABLES

LIST OF FIGURES

1. INTRODUCTION

The main Wanderer magnetic anomaly is a slightly elliptical "bull's eye" of approximate dimensions 2.2 km (E-W) x 1.8 km (N-S) with an amplitude of ~ 1400 nT and a half-width of ~ 400 m. The main anomaly lies at the eastern end of an ESE-striking magnetic horizon that has a total strike extent of ~ 4.5 km and appears to be associated with mineralised schists within the Rudall Metamorphic Complex.

Preliminary 2-1/2 D modelling of the anomaly by N. Stolz indicated that the anomaly amplitude and shape (in particular the absence of a significant low to the south of the almost symmetrical magnetic high) could be explained by a relatively deep (180 m to the top) tabular body of great depth extent, with shallow dip to the south, assuming magnetisation parallel to the Earth's field. The (SI) susceptibility-orthogonal thickness product required to account for the anomaly amplitude is approximately 28 m.

The metasedimentary units are tightly folded in this area and appear to dip steeply to the north, parallel to a well-developed axial plane schistosity. Therefore, if the magnetic source is south-dipping (as interpreted from the anomaly on the assumption that it is magnetised parallel to the Earth's field) it cannot correspond to a stratigraphic unit or units. On the other hand, if the magnetic body is bedding-parallel, the assumed magnetisation direction must be erroneous.

Two diamond holes (87WWD1 and 87WDD2) were drilled to test the anomaly. Both holes intersected magnetic material at considerably shallower depths than the interpreted source. The two intersections suggest the presence of a relatively thin and shallow magnetic horizon dipping to the north. Furthermore, the material intersected at depth by 87WDD1, which lay within the interpreted magnetic body, was only weakly magnetic.

In summary, the intersected magnetic material was consistent with a thin, shallow, concordant magnetic horizon, lying completely outside the originally interpreted magnetic source. The drilling raises the following questions:

(i) Does the intersected magnetic material account for the observed anomaly?

(ii) If so, is the misinterpreted dip due to remanent magnetisation, anisotropic susceptibility, self-demagnetisation or a combination of these factors?

(iii) If not, where is the true source of the anomaly?

The magnetic properties of ten drill core samples from 87WDD2 were studied with the aim of resolving these questions.

2. MAGNETIC PETROPHYSICS

The remanent and induced magnetisations of the drill core samples are given in Table 1. Sample no.s 1727201-208 (202 m-241 m depth) lie within the magnetic zone defined by the susceptibility log of the hole, whereas samples 1727209-210 (304 m-305 m depth) lie below it. The properties are quite variable, but the most magnetic samples exhibit fairly consistent remanence directions which are ~ S and steep up, i.e. they are quite oblique to the present field. Furthermore, the induced magnetisation is significantly deflected away from the present field direction towards the schistosity, which is a plane of higher susceptibility. The effective Koenigsberger ratio is ~ 1. The resultant magnetisation direction is ~ S and very steep up, ~ 45° from the present field. This implies that a considerable error in interpreted dip would result by assuming magnetisation parallel to the Earth's field (see Clark and Schmidt, 1986).

The magnetic carrier in the most magnetic sample (#1727203) was identified as magnetite using thermomagnetic analysis. The susceptibility-temperature curve for this sample is shown in Fig. 1. The curve is almost perfectly reversible, showing that negligible chemical change occurred during the heating.

The prominent peak at ~ -150°C corresponds to the isotropic point of pure magnetite and indicates that the susceptibility is dominated by multidomain (MD) grains, for which the intrinsic susceptibility is mainly controlled by magnetocrystalline anisotropy.

A relatively flat curve from room temperature to ~ 560°C, before the rapid descent to the Curie point, is typical of predominantly MD grains, but the gradual increase in susceptibility between 0°C and 560°C indicates a successive unblocking of grain magnetisations which is behaviour that is typical of very fine single domain (SD) particles. The thermomagnetic curve therefore demonstrates the presence of a fraction of SD grains, with a blocking temperature distribution extending from 0°C almost up to the Curie point, as well as MD grains. The SD grains with blocking temperatures well above room temperature are capable of retaining a stable, ancient and relatively intense remanence. The Curie point is ~ 580°C which confirms that the magnetite is almost stoichiometric Fe_3O_4. There is no contribution to the susceptibility from pyrrhotite or other magnetic phases.

The NRM directions of specimens from all the samples and from the three most magnetic samples are shown in Figs. 2(a) and 2(b) respectively. the plots show that there is no tendency for the NRMs to cluster around the present field direction. The NRMs of the strong samples are ~ S and steep up, whereas the weak samples tend to have the opposite polarity (NRMs ~ N and down). Overall the distribution of NRM directions suggests the presence of ancient remanence components with little overprinting by a viscous remanence (VRM) acquired subparallel to the Earth's field.

Palaeomagnetic cleaning was carried out on specimens from all samples in order to test the stability of the remanences. Representative Zijderveld plots (see Fig. 2(c) for explanation) are shown in Figs. 2(d)-2(l). These plots are described by Schmidt and Clark (1985). The closed symbols represent projections of successive remanence vector end-points onto the horizontal plane and the open symbols are the projections of the vector end-points onto a vertical plane.

Fig. 2(d) shows that specimen 205D possesses an essentially mono-component remanence, directed steeply upwards, after removal of a small amount of palaeomagnetic noise by the first AF cleaning step (5 Oe). Specimen 212B (Fig. 2(e)) exhibits similar behaviour, but the expanded view of the region around the origin (the right hand plot) shows that

the end-points are not heading directly towards the origin. This indicates the presence of a small unresolved hard component of remanence. The NRM, however, is dominated by the steep upward component, which is stable up to at least 200 Oe.

Sample 202 m has a complex magnetisation as shown by demagnetisation plots for three different specimens (Fig. 2(f)-(h)). Specimen 202A has an essentially monocomponent NRM, whereas 202B has two, approximately antiparallel, components with fairly discrete AF coercivity spectra. The "normal" (S and up) component dominates the NRM. On the other hand specimen 202C has a multicomponent NRM which is dominated by a "reversed" (N and down) component. Thermal demagnetisation fails to completely resolve the components, which have highly overlapped blocking temperature spectra, but a steep upward component appears to be isolated above 400°C.

Sample 210m exhibits intriguing behaviour. Both AF (Fig. 2(i)) and thermal (Fig. 2(j)) demagnetisation indicate the presence of antiparallel components, which are well resolved by cleaning. The NRM of 210C is dominated by the characteristic component (S and steep up) of normal polarity which is readily removed by initial AF demagnetisation to 40 Oe, revealing a more stable component of reversed polarity, which is in turn removed between 40 Oe and 60 Oe, isolating a stable component which appears to be parallel to the initially removed component. This implies that the normal component has a broad coercivity spectrum extending from <5 Oe to >300 Oe, whilst the reversed component is carried by a fraction of grains of intermediate stability with a very narrow coercivity spectrum. Specimen 210B has an NRM dominated by the reversed component, which is removed by thermal demagnetisation to 250°C, revealing a well-defined component of normal polarity.

Sample 304 m is typical of those with NRM dominated by the reversed component. Thermal demagnetisation of 304B (Fig. 2(k)) reveals an essentially monocomponent remanence directed NNW and steep down. Specimen 304A has an NRM dominated by an N down component, but AF demagnetisation reveals the presence of a minor hard component, which is not fully resolved but which appears to lie within the south-up quadrant (Fig. 2(l)).

Overall the remanence of the samples is oblique to both the present field direction and the drilling axis and appears to be a stable, ancient multicomponent magnetisation representative of the in situ remanence of the magnetite-bearing schists, rather than an artefact of drilling. Palaeomagnetic noise acquired since drilling appears negligible. The remanence tends to lie close to the schistosity plane and may have been significantly deflected by anisotropy away from the ambient field direction, towards the plane of high susceptibility, at the time of remanence acquisition. This means that estimation of the palaeofield direction for calculation of a geomagnetic pole requires correction for the effect of anisotropy.

The mean remanence direction differs significantly from the induced magnetisation direction, even allowing for the effects of anisotropy on the induced magnetisation, indicating that the NRM is not a recently acquired VRM. This conclusion is confirmed by the dual polarity of the remanence and its resistance to demagnetisation (stability to >500°C and >200 Oe in some cases). The dual polarity of the characteristic remanence direction suggests prolonged acquisition of remanence, spanning one or more reversals of the geomagnetic field. The remanence may be a thermal overprint acquired during slow post-metamorphic cooling or may be a chemical remanence associated with gradual deposition of magnetite by mineralising fluids. Taking the anisotropy into account, at least approximately, the estimated palaeofield direction is ~ N with an inclination of -75°. The corresponding palaeopole is ~ 120°E, 50°S which is consistent with remanence acquisition in the Proterozoic either at ~ 1.7 Ga or, taking the antipole, at ~ 1.2 Ga (based on the Precambrian apparent polar wander path for Australia given by Idnurm and Giddings (1987)).

3. MAGNETIC FABRIC

The susceptibility ellipsoids of the samples and various derived parameters which characterise the anisotropy are given in Table 2. Principal susceptibility axes are plotted on lower hemisphere, equal area stereonets in Figs. 3(a)-(c). Axes from all specimens are shown in Fig. 3(a), which indicates that a relatively consistently oriented magnetic fabric is exhibited by all samples, weak and strong. The magnetic foliation (plane of relatively high susceptibility) contains the maximum and intermediate susceptibility axes and, by definition, is perpendicular to the minimum axes (the magnetic foliation poles). The magnetic lineation is defined by the grouping of maximum susceptibility axes. The plots indicate generally N-plunging magnetic lineations, within a steeply N-dipping magnetic foliation that is parallel to the schistosity.

The corresponding plots (Fig. 3(b)) for the most magnetic samples (from 210 m to 212 m) show well-clustered susceptibility axes that indicate a lineation plunging to the north within a north-dipping schistosity-parallel magnetic foliation. The degree of anisotropy is very high, and is the reason for the significant deflection of the induced magnetisation from the present field direction that is evident from Table 1. The overall anisotropy is 2.3 in the magnetic zone and is somewhat lower (A = 1.67) outside this zone. The susceptibility ellipsoids are triaxial and the magnetic foliation is slightly stronger than the lineation ($P<1$, $t>1$) within the magnetic zone, but is considerably weaker ($P>1$, $t<1$) than the lineation outside the zone. Fig. 3(c) shows plots of various anisotropy parameters for the most magnetic samples. The ellipsoid shape and anisotropy degree are almost independent of the bulk susceptibility.

The strength of the magnetic fabric requires a very high degree of preferred orientation of elongated magnetite grains and/or an arrangement of magnetite into discrete highly magnetic sheets within which grains tend to be strung out along the lineation. The magnetic lineation probably reflects the direction of maximum extension associated with the deformation of these rocks.

The samples near the bottom of the hole, below the intersected magnetic zone have a somewhat different magnetic fabric. The axes are not as well grouped as for the more magnetic samples and the maximum and intermediate axes are approximately interchanged with respect to the magnetic zone. The magnetic lineation for the samples from 304 m and 305 m is E-plunging and the magnetic foliation is somewhat rotated, dipping to the NE rather than north (see Fig. 3(d). This may reflect different styles of deformation within and outside the mineralised zone. The change in orientation of the magnetic foliation down the hole also suggests some refolding of the fabric developed during the intense deformational (and mineralising?) event.

4. MAGNETIC MODELLING

An attempt to model the Wanderer anomaly was made using a thin tabular body that was fitted to the magnetic intersections in the two drill holes and assumed to extend to great depth. For simplicity 2D modelling was used. This model (model 1 in Fig. 4) represents an apparently conformable mineralised zone with properties assumed to be consistent with those of the samples from the magnetic zone intersected by 87WDD2. Because the magnetisation of the rocks outside the magnetic zone is not negligible, the magnetisation contrast of the magnetic zone with the surrounding material was calculated (see Table 1) and used in modelling.

Fig. 4 shows the observed ground magnetic anomaly, the drill holes and magnetic intersections, and two models with their corresponding calculated anomalies. Although the anomaly amplitude can be explained by model 1 the theoretical anomaly is much narrower and has a more prominent low to the south than the observed anomaly. Clearly, the observed anomaly is not satisfactorily explained by a simple geometric interpretation of the drill hole intersections. Modifications of the model to allow for finite strike length and depth extent only exacerbates the poor fit between calculated and observed anomalies.

Model 2 represents a source for which the calculated and observed anomalies agree satisfactorily, given the approximation introduced by the assumption of infinite strike extent. The body is assumed to

consist of similar material to that intersected by 87WDD2 and is assigned the same magnetic properties as Model 1. Model 2 can be considered equivalent to the initial model of N. Stolz, which was discussed in the introduction, with correction for the difference between the resultant magnetisation direction and the Earth's field direction. This difference, which reflects both the remanence and the anisotropy (in about equal measures), essentially accounts for the large difference in interpreted dip (70°S instead of 35°S) between the model 2 and the initial model, which assumed magnetisation parallel to the present field. There is also a small effect on the interpreted dip (~ 10°) due to the assumption of infinite strike extent. The dip of a 2-1/2 D equivalent model is ~ 80°S.

Although model 2 gives a reasonable match to the observed anomaly, it does not fit the drilling data. The ~ 75 m within model 2 which was intersected by 87WDD2 is only weakly magnetic. This suggests that the main source of the anomaly lies at greater depth. Modelling the geometry of this deep source requires an evaluation of the effect of the shallow magnetic material, intersected in the drill holes, on the total anomaly. Fig. 5 shows calculated anomalies for simple 2D polygonal models which fit the drilling intersections. Even with the most conservative assumptions about the extent of the magnetic zone, a substantial (>600 nT), asymmetric anomaly of half width ≈ 150 m, which would noticeably perturb the northern flank of the broad, symmetric main anomaly, is predicted. There is no evidence in the observed signature of such a pronounced effect from the shallow magnetic material, implying that the intersected magnetic zone must have very limited strike extent and be quite discontinuous.

Model 3 of Fig. 6 is an attempt to explain the observed signature using a single 2D body, consisting of a steeply S-dipping sheet of great depth extent joined to the shallow magnetic zone, which also fits the drilling intersections. The theoretical anomaly is much narrower than the observed anomaly. Subtraction of the model 3 anomaly from the observed data leaves a residual anomaly consisting of two distinct broad peaks, which would require at least two further sources of very specific geometry and properties to explain them. Although the anomaly could in principle be explained by a complex source, consisting of multiple

bodies, which happened to produce a signature resembling that of a simple tabular body, such a circumstance is extremely improbable. Thus ad hoc modelling of the anomaly by a complex source which has been forced to fit the drilling data is unjustifiable.

The most parsimonious interpretation of the data appears to be, therefore, a deep, unintersected, simple body which accounts for the anomaly. The intersected shallow magnetic material must represent discontinuous, strike-limited magnetic zones producing negligible magnetic response at the surface. Such a model is shown in Fig. 6 (model 4). The anomaly can only be satisfactorily matched by a deep body, lying below the drill holes, if it has limited depth extent. Semi-infinite sheets producing equivalent matches to the anomaly are required to have depth to top less than 200-250 m and should have been intersected by the drilling. Further modelling with varying depth extents indicates that the anomaly can be matched by a body at depth of approximately 300 m, or slightly greater, provided the depth extent falls in the range ~ 600 m to ~ 1500 m. Allowing for finite strike length would increase slightly the estimated depth and the permissible depth extent. The interpreted magnetic source is therefore a major deep body, which would nevertheless be accessible by drilling if further testing of the anomaly were judged to be necessary.

5. SUMMARY AND CONCLUSIONS

1. The magnetic schists intersected by DDH 87WDD2 are highly anisotropic (A ~ 2.3) and carry a stable, ancient remanence of dual polarity which is oblique to the present field direction. The only important magnetic mineral is MD plus SD pure magnetite. The remanence is predominantly of normal polarity and is directed S and steeply upward. The Koenigsberger ratio is ~ 1 and the resultant magnetisation differs from the Earth's field direction by ~ 45°. The remanence direction is consistent with acquisition either at ~ 1.7 Ga or ~ 1.2 Ga.

2. The magnetic fabric is well-defined with a N-NE dipping magnetic foliation parallel to the schistosity. Within the magnetic foliation there is a pronounced lineation, generally plunging to the north, which may represent the direction of maximum extension.

3. The obliquity of the resultant magnetisation direction of the schists with respect to the present field could produce significant errors in interpreted dips for sheet-like geometries. For an E-W strike the dip interpreted assuming magnetisation parallel to the Earth's field would be swung ~ 45°S from the true dip.

4. Modelling reveals that the Wanderer anomaly cannot be explained by the magnetic material intersected in the drill holes, although a persistent horizon of such material would produce a prominent narrow anomaly. The absence of a sharp signature superimposed on the broad anomaly implies that the intersected magnetic zone is discontinuous and very strike limited.

5. The broad anomaly is due to a relatively deep body which does not appear to have been intersected. Assuming the main magnetic body reflects the same pronounced schistosity and magnetic history, and can be assumed to have similar magnetic properties as the intersected magnetic zone, a dip of 70°S-80°S is indicated by the anomaly. The preferred interpretation of the Wanderer magnetics attributes the anomaly to a major body, somewhat deeper than the drill holes, with estimated parameters: depth to top ~ 300 m; dip 70°S-80°S; horizontal width 210 m; depth to bottom ~ 1300 m; magnetisation contrast 1350γ, dec = 198°, inc = -80°.

6. REFERENCES

Clark, D.A. and Schmidt, P.W., 1986. Geological structure and magnetic signatures of Hamersley BIFs. CSIRO Restricted Investigation Report 1639R.

Idnurm, M. and Giddings, J., 1987. Australian Precambrian apparent polar wander : a review. Tectonophysics (in press).

Schmidt, P.W. and Clark, D.A., 1985. Presentation and analysis of palaeomagnetic data. CSIRO Restricted Investigation Report 1602R.

TABLE 1 MAGNETISATION OF SAMPLES FROM DDH 87WDD2

Sample	Depth	N	$\tilde{J}_{NRM}$	$\tilde{J}_{IND}$	$\tilde{J}_{RES}$	Q
1727201	202 m	3	(307;185°,-68°)	(886;333°,-65°)	(1124;321°,-75°)	0.35
1727202	205 m	5	(49;87°,-69°)	(470;2°,-57°)	(510;6°,-60°)	0.10
1727203	210 m	4	(3305;181°,-54°)	(2168;24°,-82°)	(5101;177°,-71°)	1.5
1727204	212 m	3	(2170;159°,-67°)	(683;47°,-78°)	(2784;150°,-73°)	3.2
1727205	226 m	5	(47;11°,+40°)	(95;344°,-72°)	(88;359°,-43°)	0.49
1727206	231 m	4	(1;47°,-57°)	(4;356°,-59°)	(5;6°,-60°)	0.25
1727207	234 m	4	(127;1°,+17°)	(434;327°,-66°)	(459;341°,-52°)	0.29
1727208	241 m	4	(231;229°,-29°)	(1505;308°,-67°)	(1635;290°,-66°)	0.15
1727209	305 m	5	(34;323°,+77°)	(53;352°,-66°)	(32;345°,-28°)	0.64
1727210	304 m	3	(135;81°,+37°)	(175;333°,-58°)	(136;33°,-30°)	0.77
All samples		10	(568;175°,-60°)	(632;342°,-75°)	(1110;192°,-83°)	0.90
(A) Magnetic zone (1727201-208)		8	(723;177°,-61°)	(763;342°,-75°)	(1380;195°,-83°)	0.95
(B) Background (1727209-210)		2	(77;77°,+48°)	(114;337°,-60°)	(81;24°,-31°)	0.68
Magnetisation contrast:(A)-(B)			(779;185°,-62°)	(654;344°,-78°)	(1350;197°,-80°)	1.2

N = no. of magnetisation vectors combined to calculate mean

$\tilde{J}_{NRM}$ = natural remanent magnetisation vector

$\tilde{J}_{IND}$ = induced magnetisation vector

$\tilde{J}_{RES}$ = resultant magnetisation vector = $\tilde{J}_{NRM} + \tilde{J}_{IND}$

Magnetisation vectors are expressed in the form: (Intensity (Y); declination, inclination). Declination is measured positive clockwise from magnetic north, inclination is measured positive downwards from the horizontal plane.

Q = Koenigsberger ratio = J_{NRM}/J_{IND}

TABLE 2 SUSCEPTIBILITY ANISOTROPY OF DDH 87WDD2 SAMPLES

Sample	Susceptibility ellipsoid (k_i; D_i; I_i)	Bulk susceptibility	A	L	F	P	t
1727201	35,720;027°,45 24,650;296°,01° 14,430;204°,45°	24,930	2.48	1.45	1.71	0.85	0.18
1727202	9770;358°,48° 9280;268°,00° 8750;177°,42°	9270	1.12	1.05	1.05	0.99	0.06
1727203	80,530;004°,57° 49,520;267°,05° 28,240;174°,33°	52,760	2.85	1.63	1.75	0.93	0.07
1727204	23,410;356°,59° 14,340;254°,07° 8,270;160°,30°	15,340	2.83	1.63	1.73	0.94	0.06
1727205	3010;042°,52° 1890;285°,20° 1450;182°,31°	2120	2.08	1.59	1.31	1.22	-0.27
1727206	78.5;080°,48° 73.1;308°,32° 65.5;201°,25°	72.4	1.20	1.07	1.12	0.96	0.21
1727207	13,680;082°,36° 10,560;317°,38° 6,340;198°,32°	10,190	2.16	1.30	1.66	0.78	0.33
1727208	48,670;059°,54° 29,580;311°,13° 17,650;212°,33°	31,960	2.76	1.65	1.68	0.98	0.02
1727209	1160;085°,65° 1080;287°,24° 750;193°,08°	1,000	1.54	1.07	1.45	0.74	0.70
1727210	4270;102°,43° 2790;342°,28° 2400;231°,34°	3,150	1.78	1.53	1.16	1.31	-0.47
All samples	21,270;025°,55° 14,590,285°,07° 9,380;190°,34°	15,080	2.27	1.46	1.56	0.94	0.08
(A) Magnetic zone	26,050;023°,55° 17,630;284°,06° 11,310;190°,34°	18,330	2.30	1.48	1.56	0.95	0.06
(B) Background	2700;101°,44° 1900;322°,38° 1620;214°,22°	2,075	1.67	1.42	1.17	1.22	-0.38
Susceptibility contrast	23,840;020°,54° 15,440;281°,07° 9,450;186°,35°	16,260	2.51	1.54	1.63	0.95	0.06

Susceptibility ellipsoids are expressed in the form: Major axis, Intermediate axis, Minor axis

Susceptibilities are given in μG/Oe (i.e. k = cgs (emu) susceptibility x 10^6)

k_i (i = 1,2,3) = major, intermediate, minor susceptibilities ($k_1 > k_2 > k_3$)

D_i = declination of i^{th} susceptibility axis, I_i = inclination of i^{th} susceptibility axis

$\bar{k}$ = bulk susceptibility = $(k_1 + k_2 + k_3)/3$

A = anisotropy parameter = k_1/k_3

L = lineation strength = k_1/k_2

F = foliation strength = k_2/k_3

P = prolateness = L/F (P > 1 : prolate ellipsoid, lineation dominant; P < 1 : oblate ellipsoid, foliation dominant)

t = 2 $[(\ln k_2 - \ln k_3)/(\ln k_1 - \ln k_3)]-1$, ($-1 \leq t \leq 1$; t > 1: oblate ellipsoid; t < 1: prolate ellipsoid)

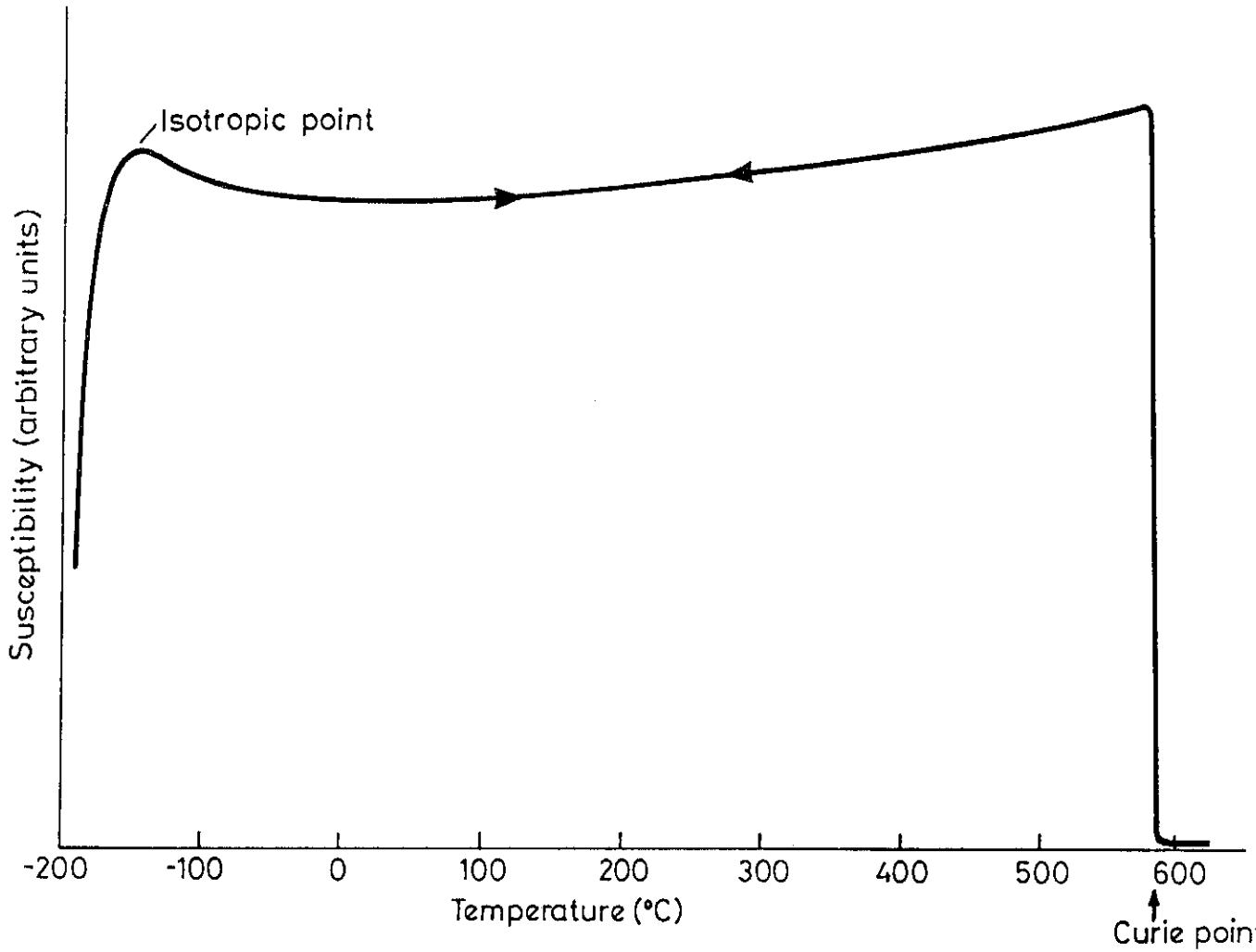

FIG. 1 LOW-FIELD THERMOMAGNETIC CURVE FOR SAMPLE DDH 87 WDD2 (210 m)

a: rudall.rem NRM

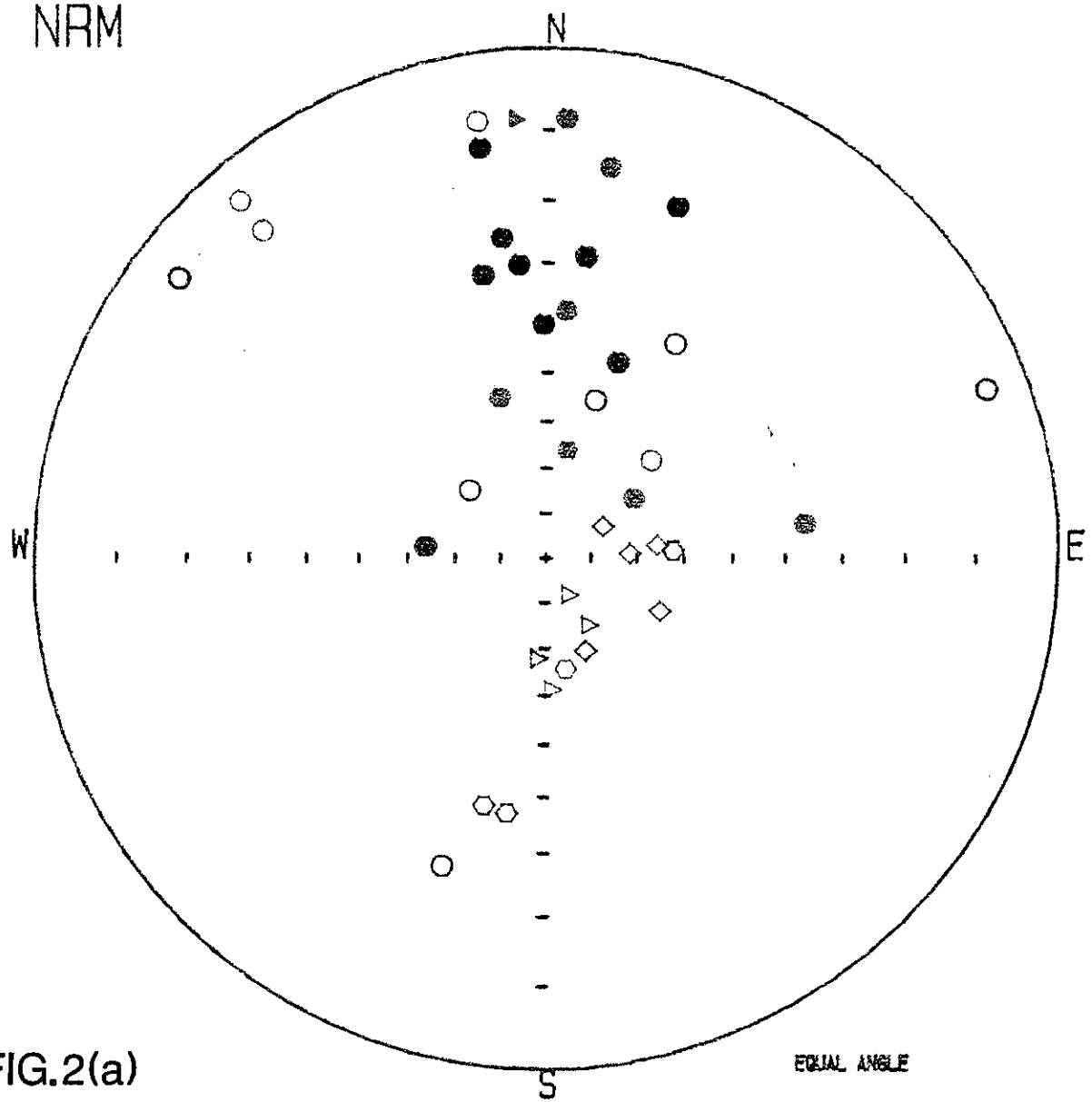

FIG.2(a)

rudall.rem

NRM

202
212
210

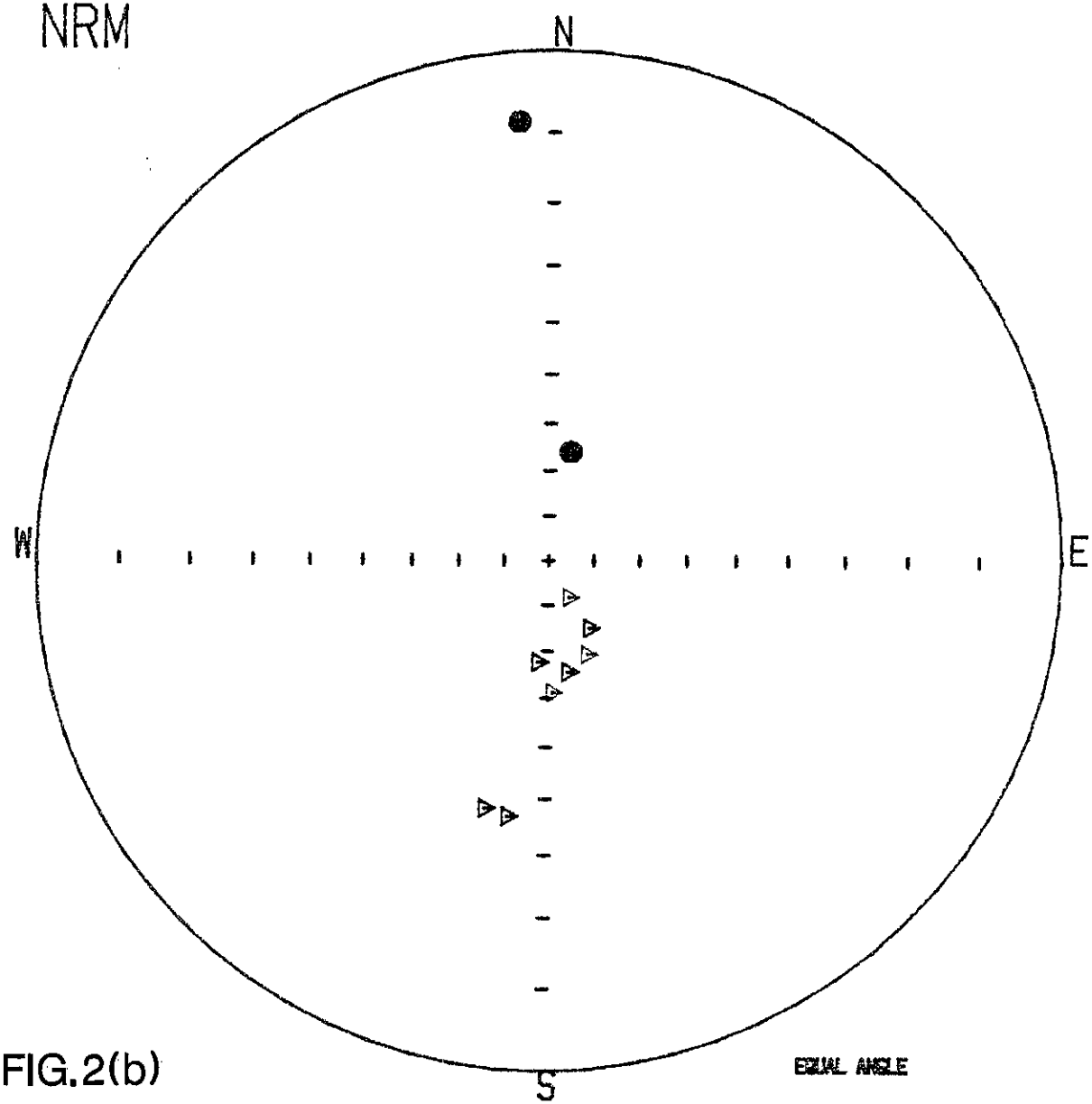

FIG.2(b)

Magnetisation is a three dimensional vector quantity and difficulties arise when representing such on a flat surface. Two separate figures are required to display a three dimensional vector. Stereographic plots and an intensity decay curve have been very useful, especially when the direction of the cleaned magnetisation is of paramount importance. However, when an appreciation of the full vectorial nature of a magnetisation is required, orthogonal projections (Zijderveld, 1967) provide an ideal method of combining both the magnitude and directional information. This greatly assists the recognition and identification of multi-component magnetisations.

(a) This illustration portrays the magnetisation decay during eight demagnetisation steps, from an oblique perspective (southeast-up octant). $\tilde{J}_1 - \tilde{J}_2$ represents the vector difference between the first and second demagnetisation step, i.e. the magnetisation removed during the second step.

(b) By simply plotting the vector end-points the diagram is greatly clarified and a soft $(\tilde{J}_s)$ and hard $(\tilde{J}_h)$ magnetisation are evident, yet a unique identification of the direction or intensity of either is not possible from this single figure.

(c) Linear combination of magnetisations yields a resultant NRM $(\tilde{J}_o)$.

(d) By projecting vector end-points onto the horizontal plane and a vertical plane allows the composition of the magnetisation to be visualised.

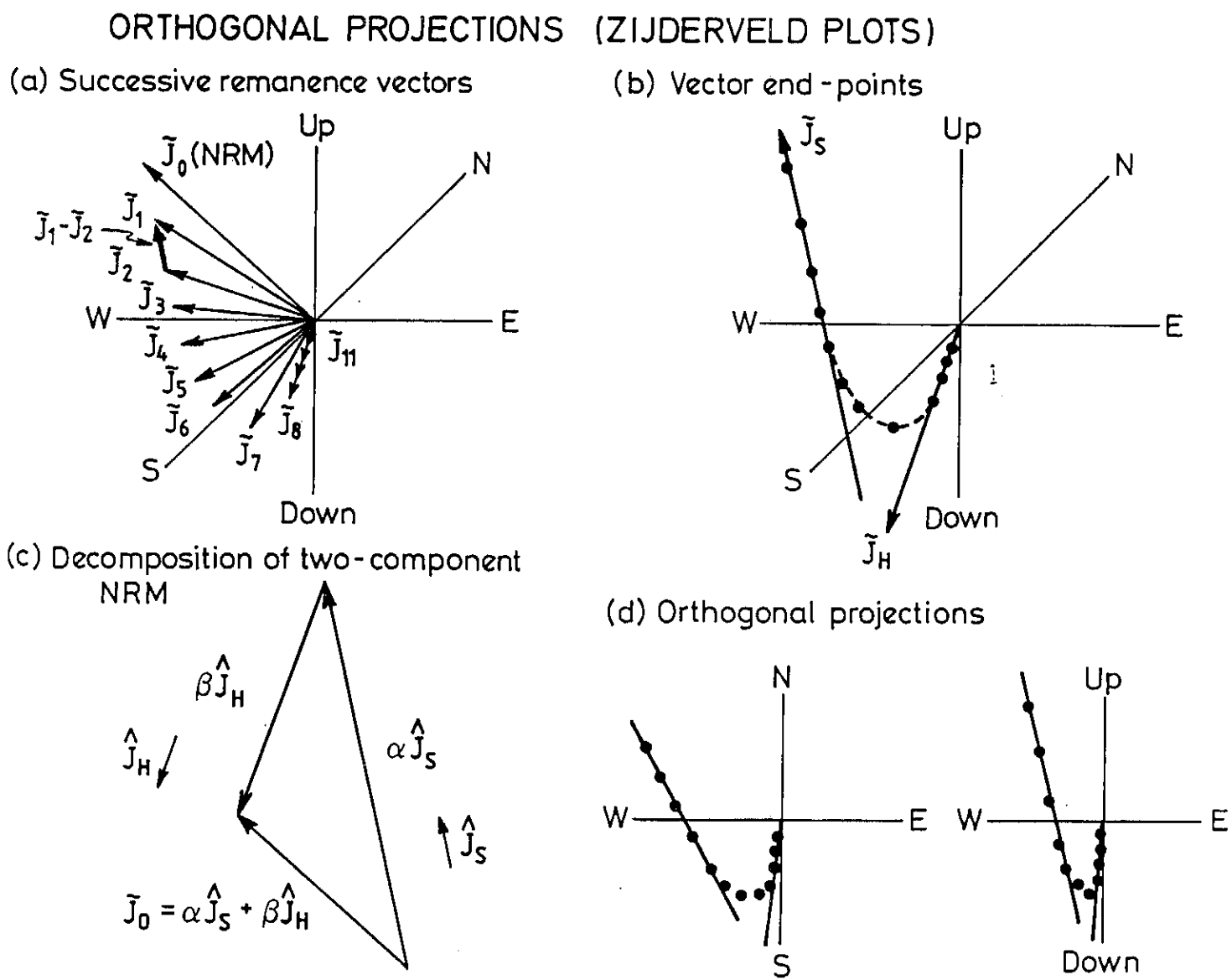
ORTHOGONAL PROJECTIONS (ZIJDERVELD PLOTS)
(a) Successive remanence vectors
Up
N
W
E
S
Down
$\tilde{J}_0$(NRM)
$\tilde{J}_1$
$\tilde{J}_1-\tilde{J}_2$
$\tilde{J}_2$
$\tilde{J}_3$
$\tilde{J}_4$
$\tilde{J}_5$
$\tilde{J}_6$
$\tilde{J}_7$
$\tilde{J}_8$
$\tilde{J}_{11}$
(b) Vector end-points
$\tilde{J}_S$
$\tilde{J}_H$
(c) Decomposition of two-component NRM
$\beta\hat{J}_H$
$\alpha\hat{J}_S$
$\hat{J}_H$
$\hat{J}_S$
$\tilde{J}_0 = \alpha\hat{J}_S + \beta\hat{J}_H$
(d) Orthogonal projections

FIG.2(c)

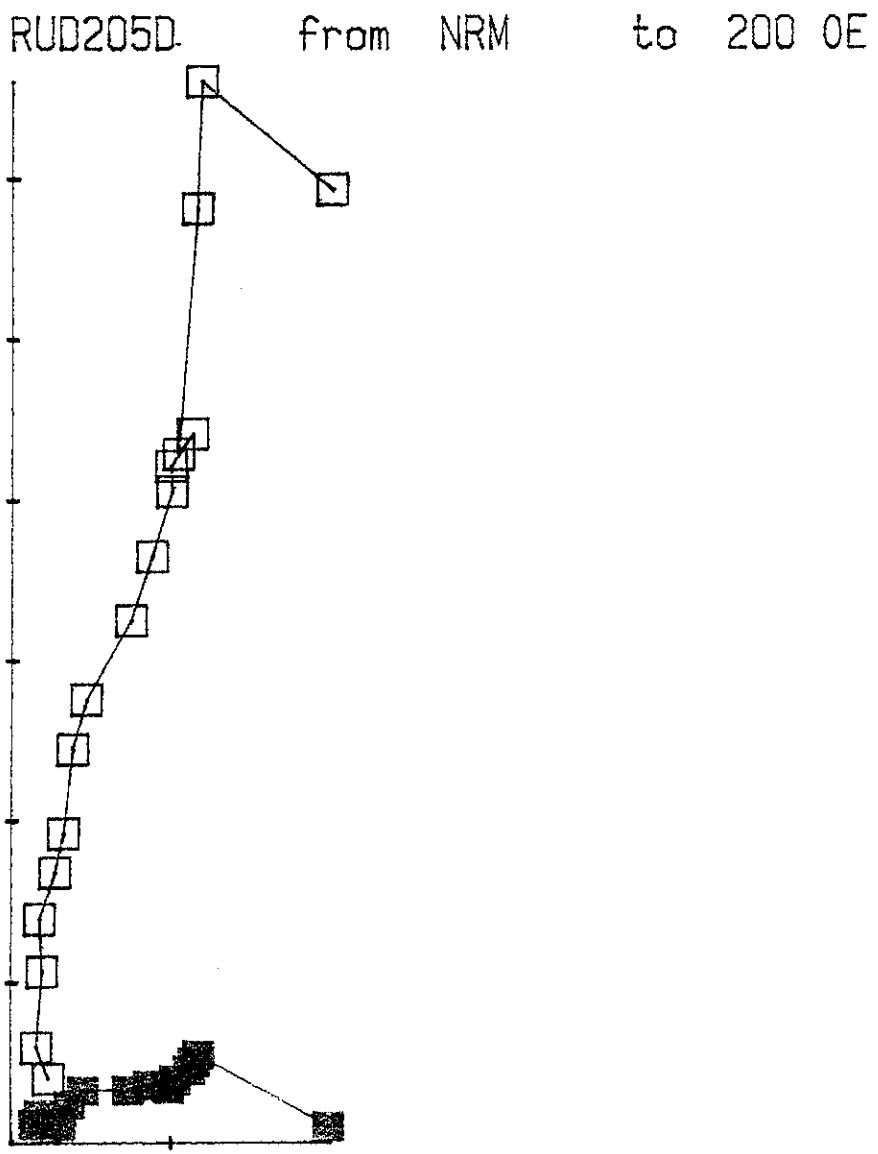

FIG.2(d)


RUD212B from NRM to 200 0E
down east
tick value is 1 * 10e3

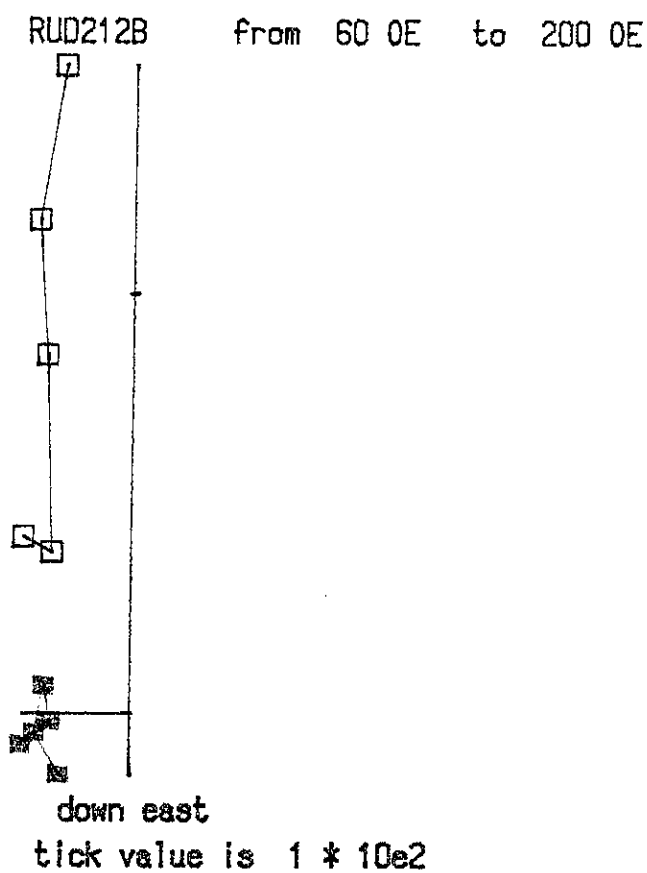
RUD212B from 60 0E to 200 0E
down east
tick value is 1 * 10e2

FIG.2(e)

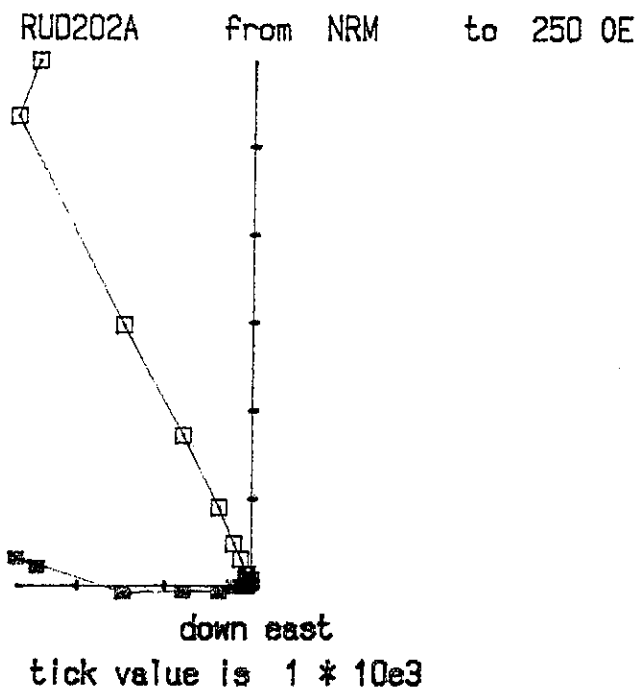
RUD202A from NRM to 250 0E
down east
tick value is 1 * 10e3

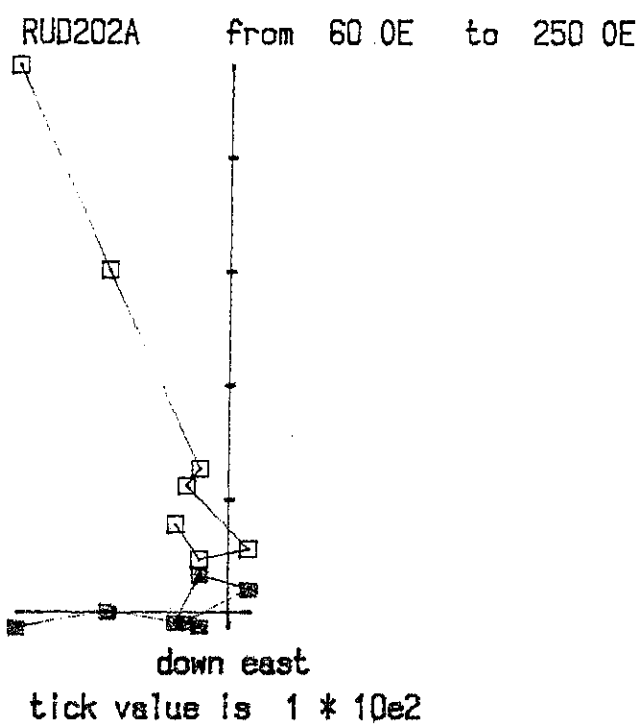
RUD202A from 60 0E to 250 0E
down east
tick value is 1 * 10e2

FIG.2(f)

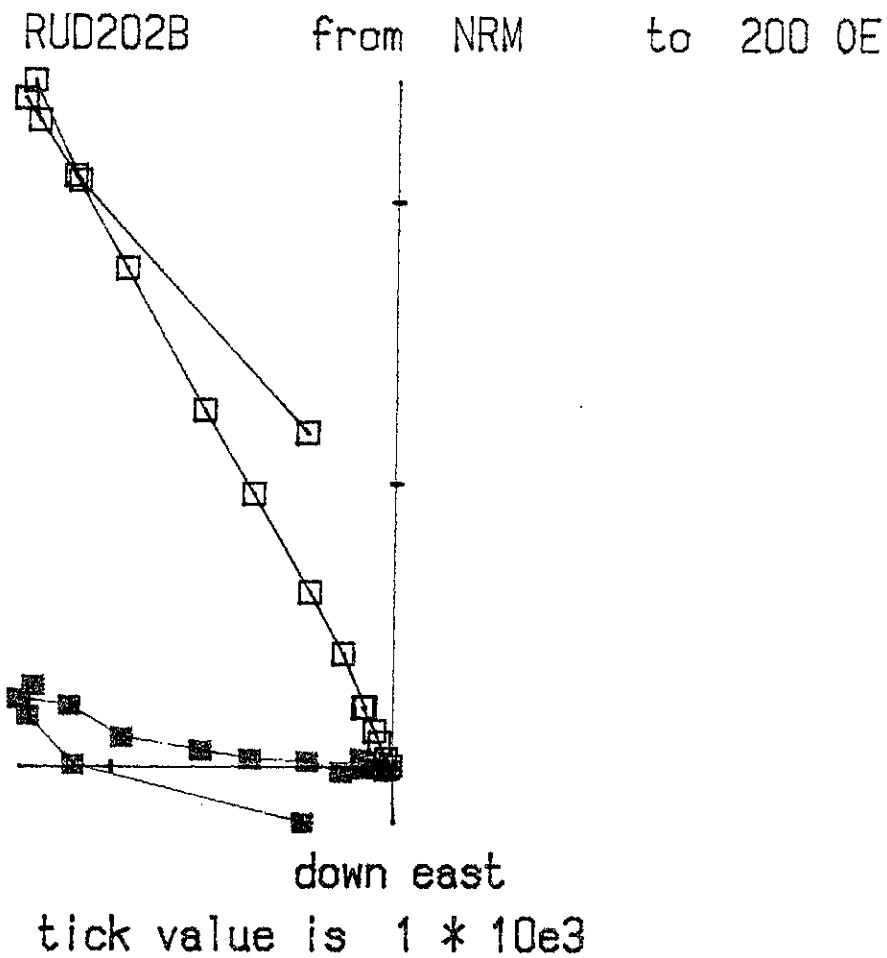

FIG.2(g)

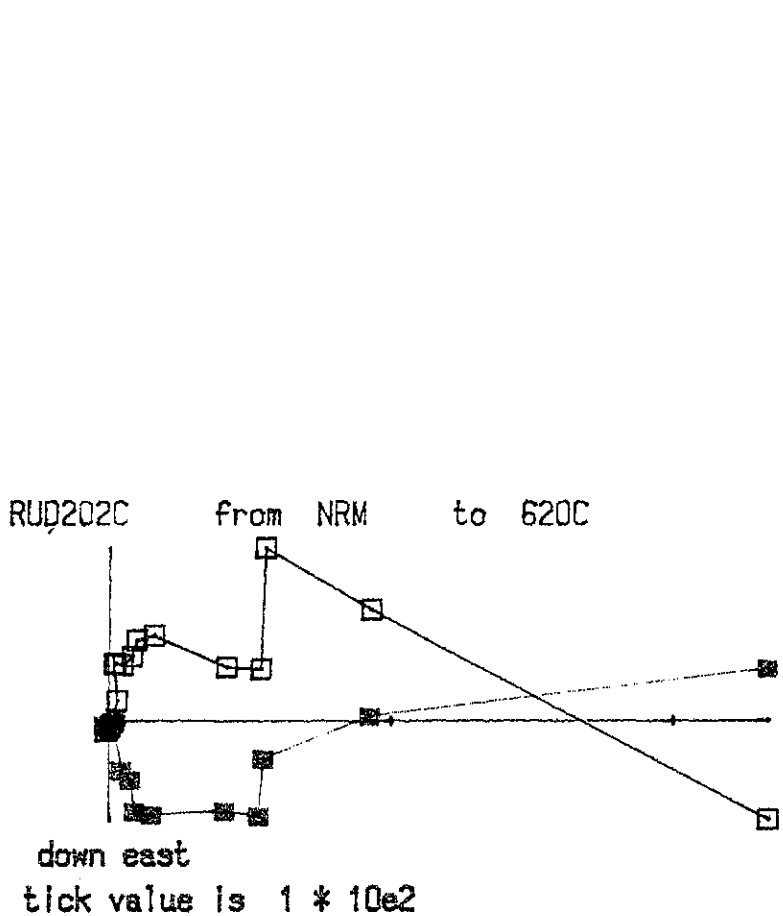
RUD202C from NRM to 620C
down east
tick value is 1 * 10e2

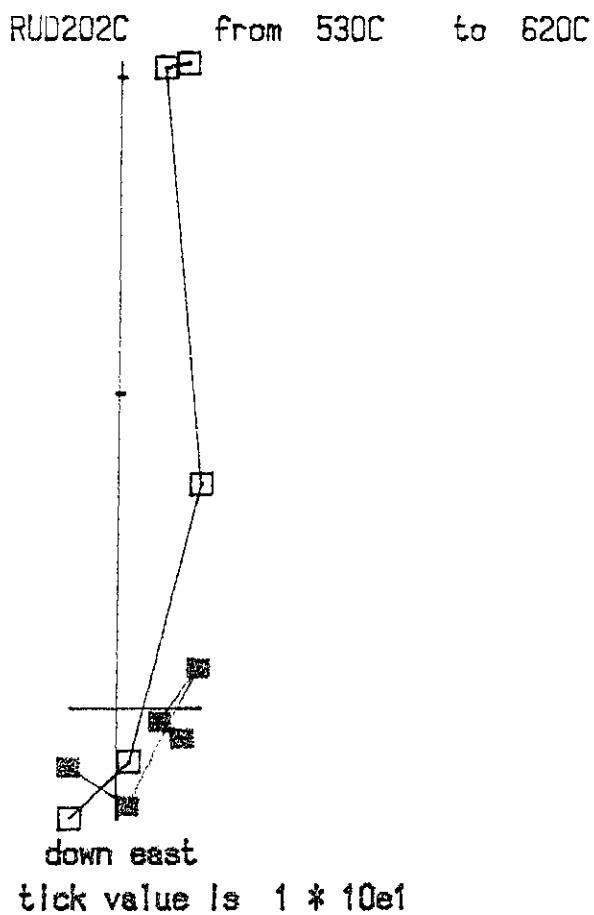
RUD202C from 530C to 620C
down east
tick value is 1 * 10e1

FIG.2(h)

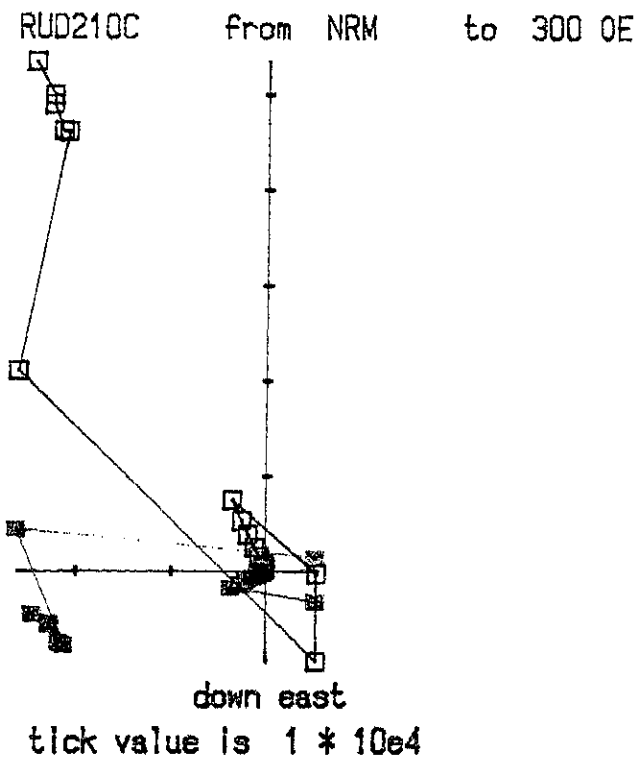
RUD210C from NRM to 300 0E
down east
tick value is 1 * 10e4

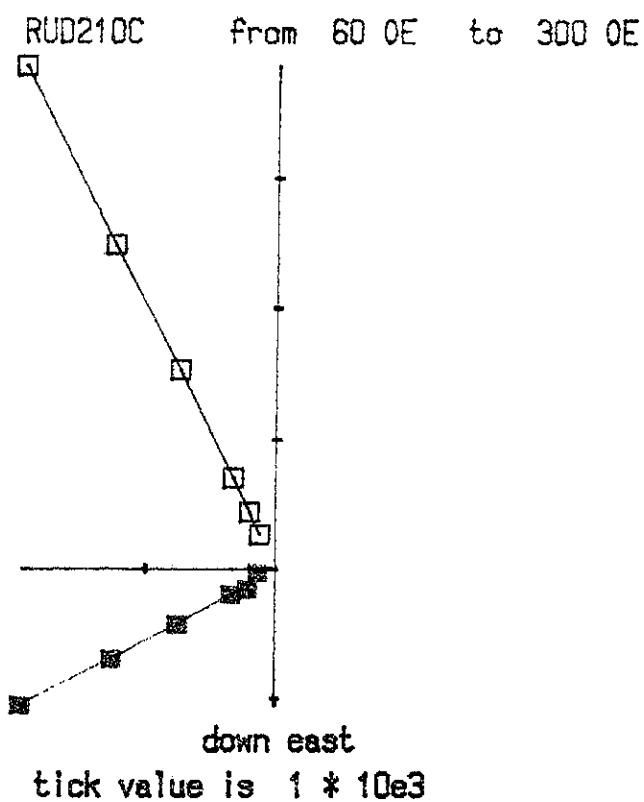
RUD210C from 60 0E to 300 0E
down east
tick value is 1 * 10e3

FIG.2(i)

RUD210B from NRM to 620C

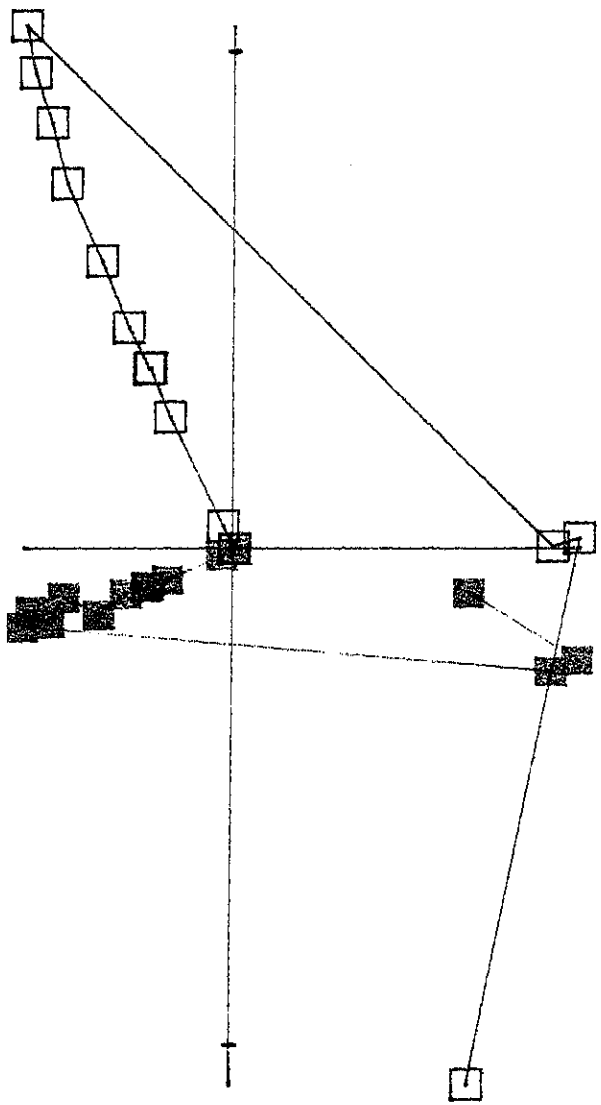

down east

tick value is 1 * 10e4

FIG.2(j)

RUD304B from NRM to 620C

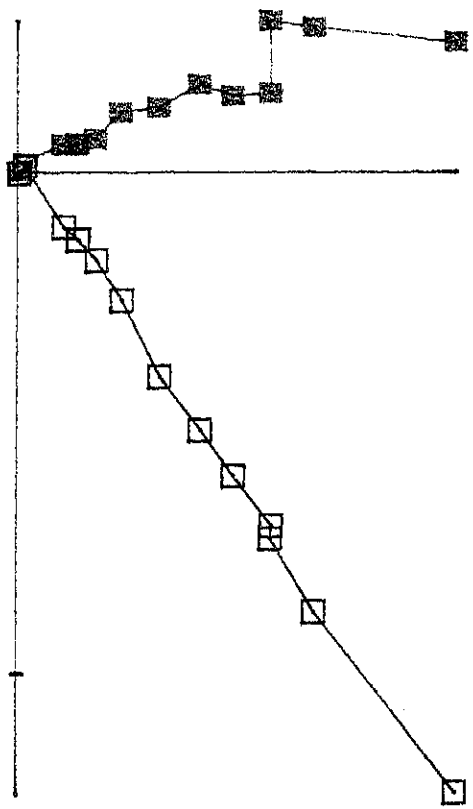

down east

tick value is 1 * 10e2

FIG.2(k)

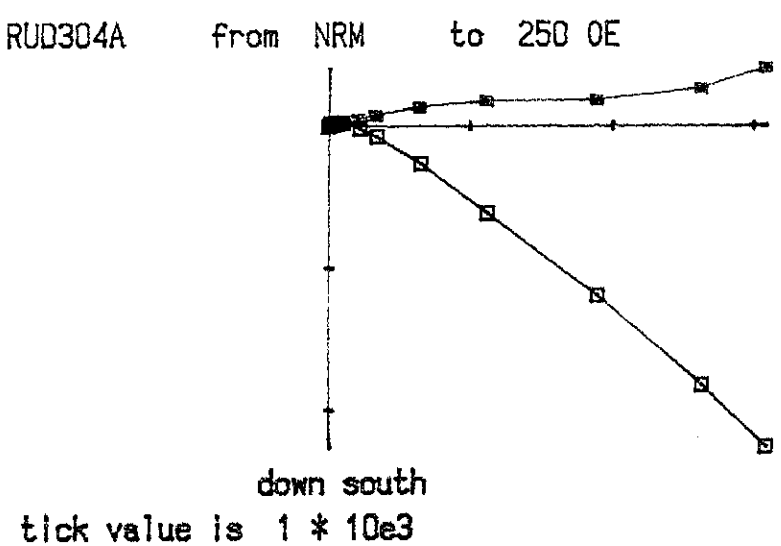
RUD304A from NRM to 250 0E
down south
tick value is 1 * 10e3

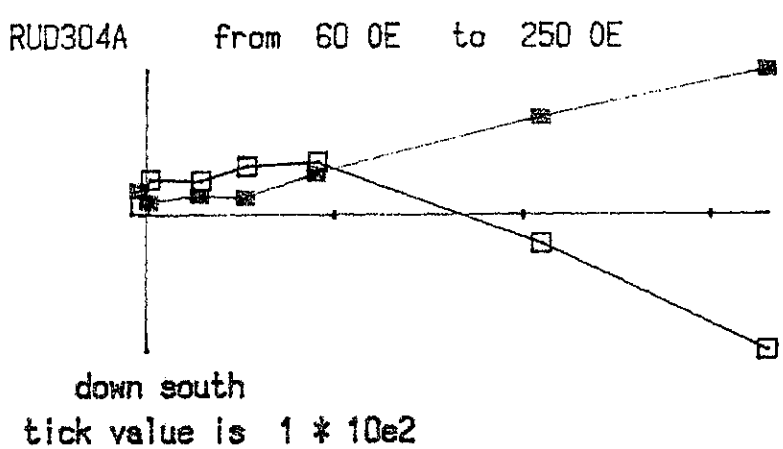
RUD304A from 60 0E to 250 0E
down south
tick value is 1 * 10e2

FIG.2(I)

A: RUDALL . sus

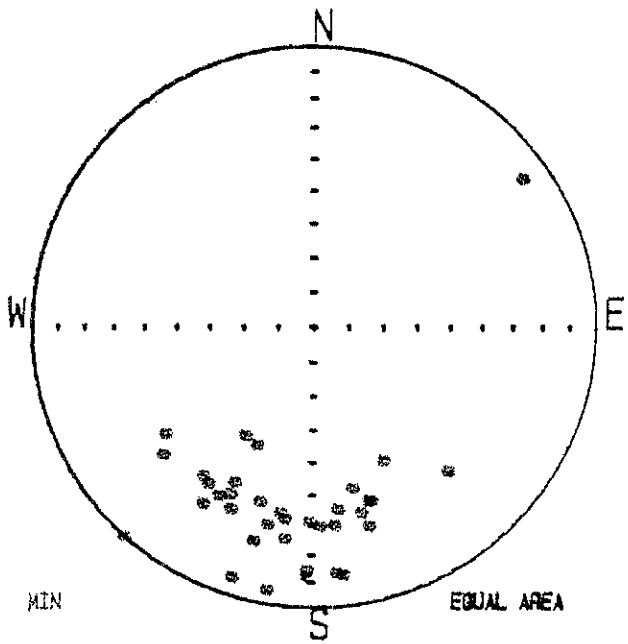

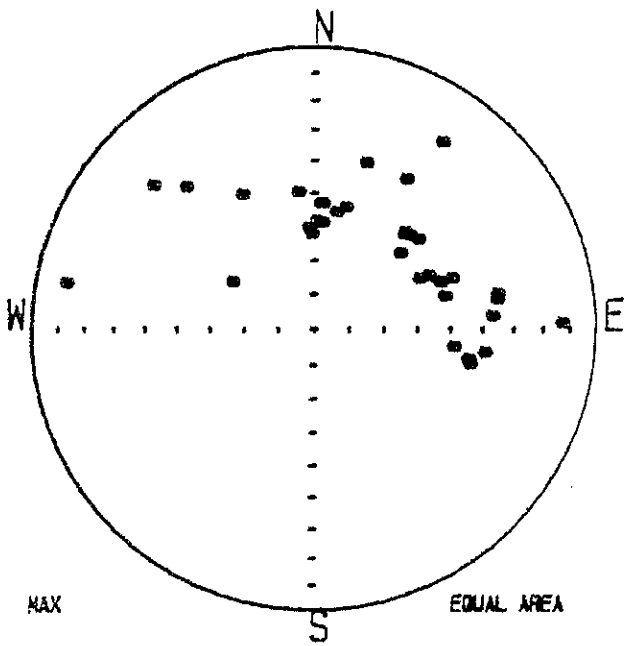

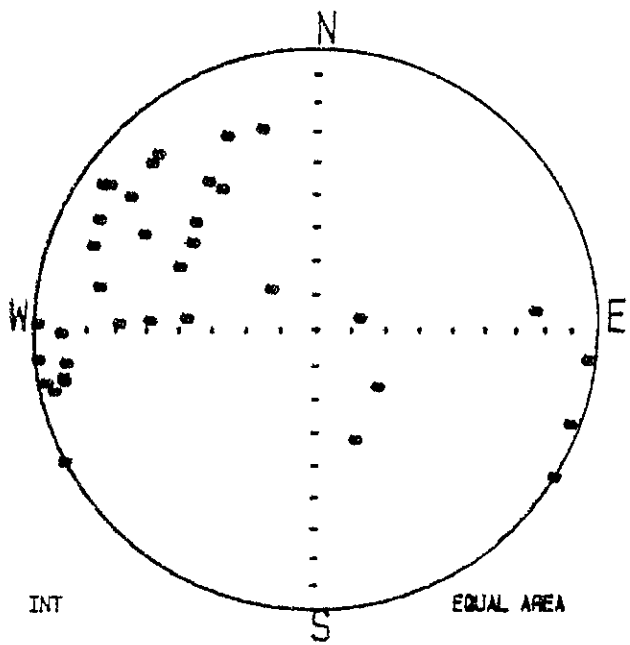

FIG.3(a)

rudall.sus

210 212

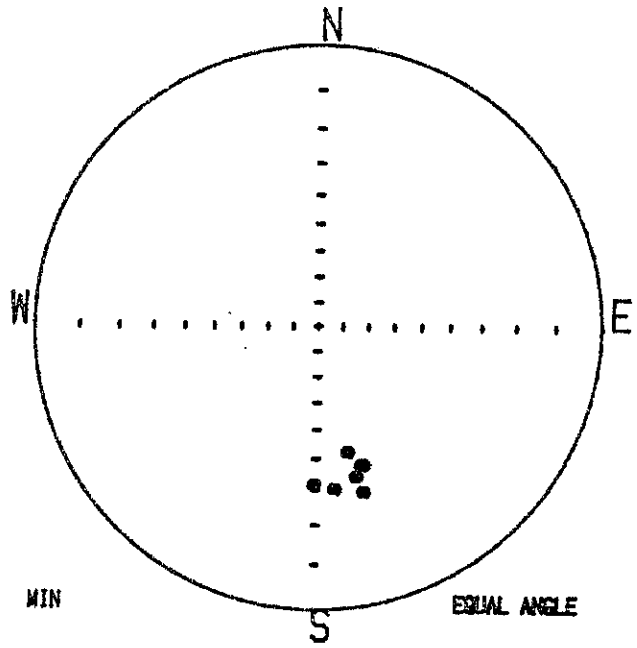

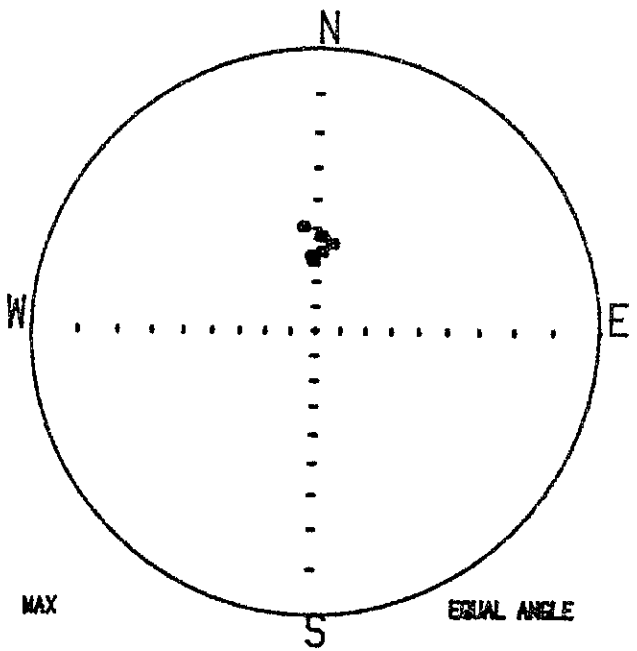

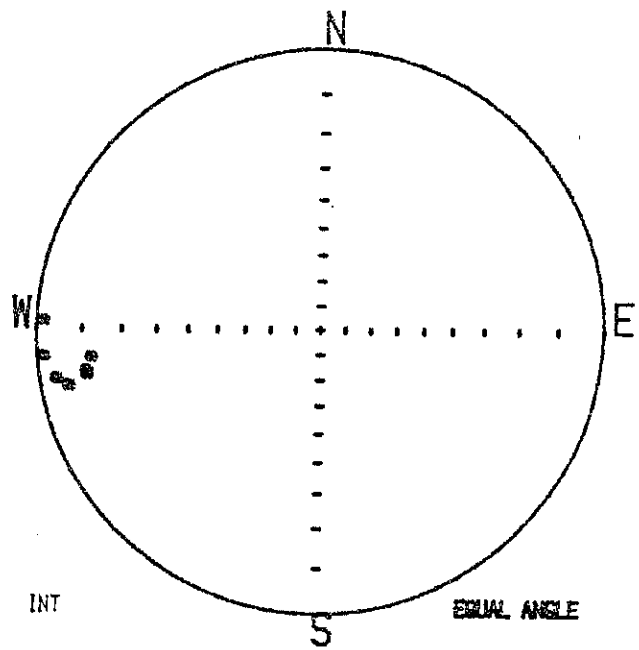

FIG.3(b)

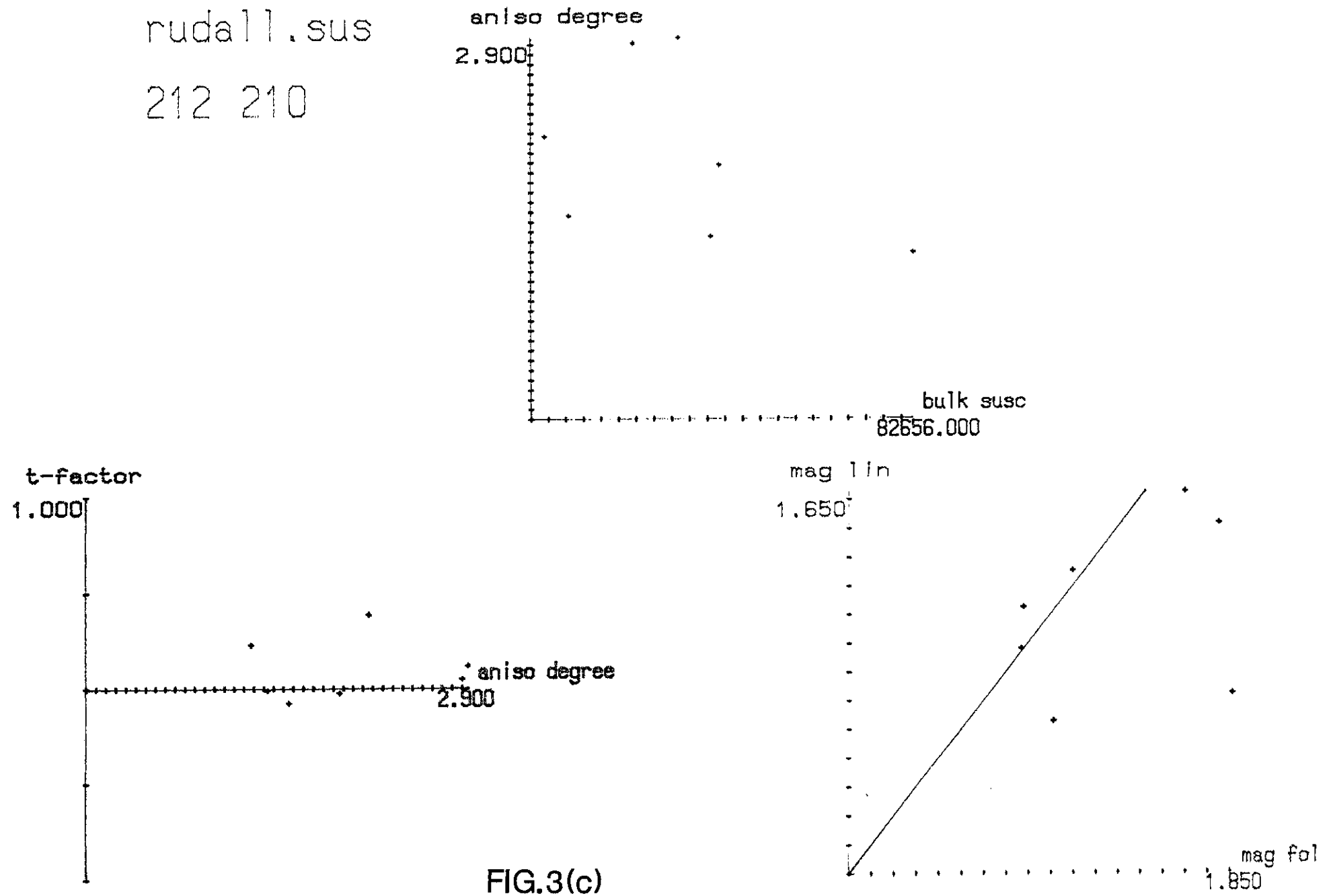
rudall.sus
212 210
aniso degree
2.900
bulk susc
82656.000
t-factor
1.000
aniso degree
2.900
mag lin
1.650
mag fol
1.850

FIG.3(c)

A: RUDALL.sus

304 305

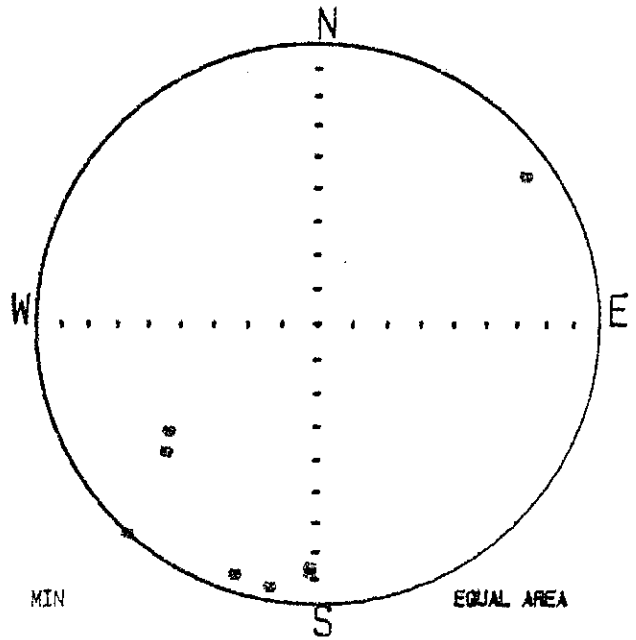

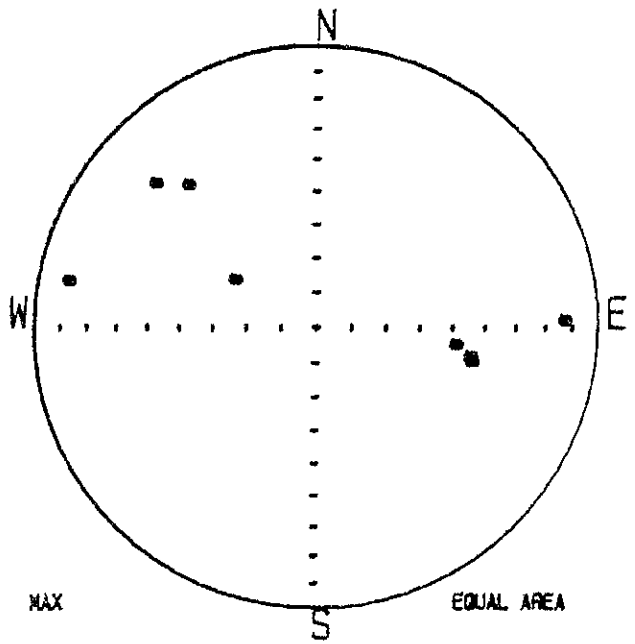

FIG.3(d)

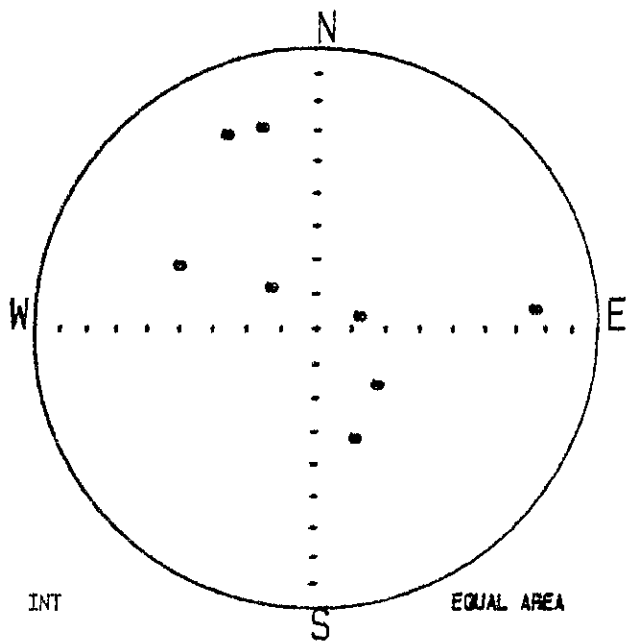

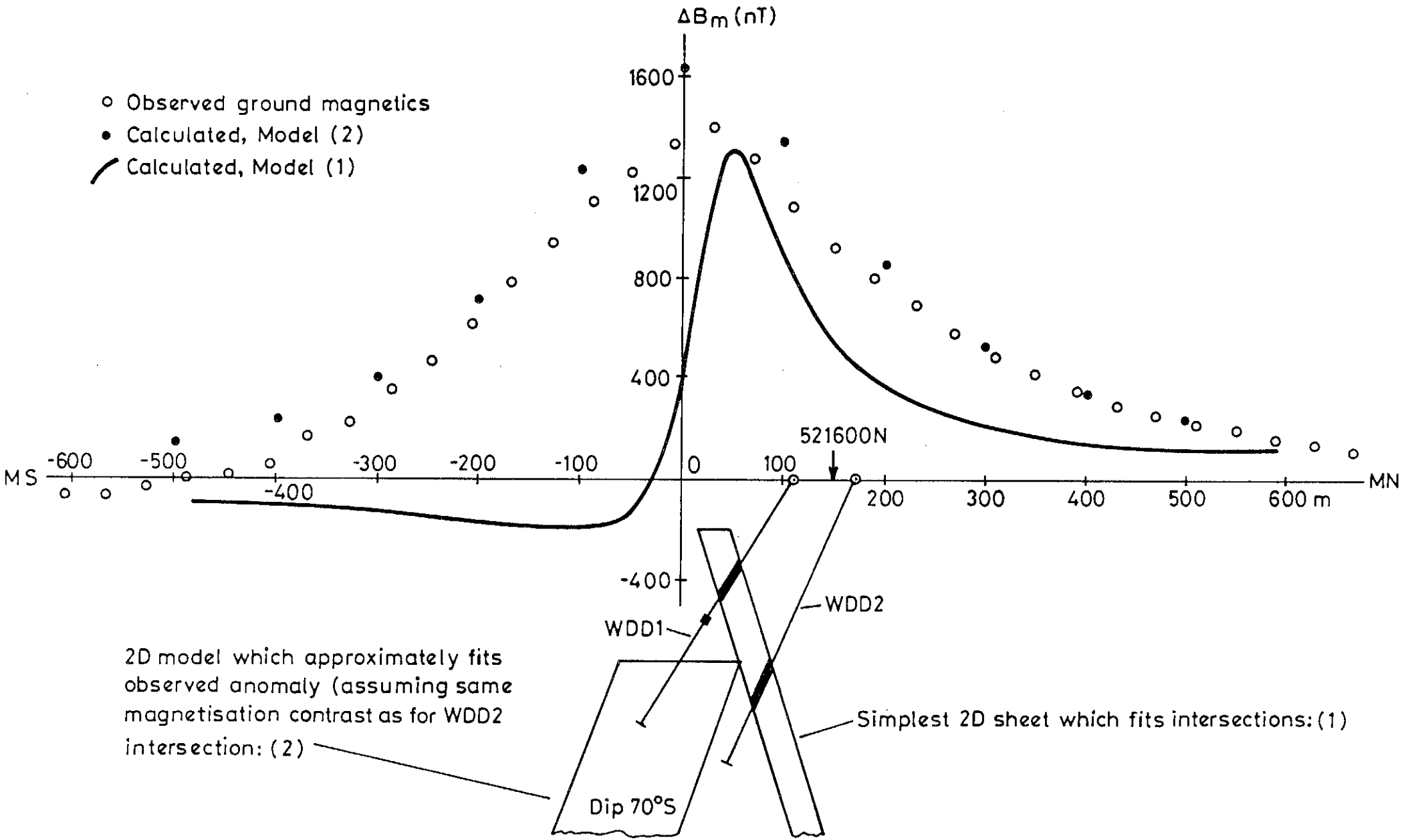

FIG. 4 MODELS OF WANDERER MAGNETIC ANOMALY

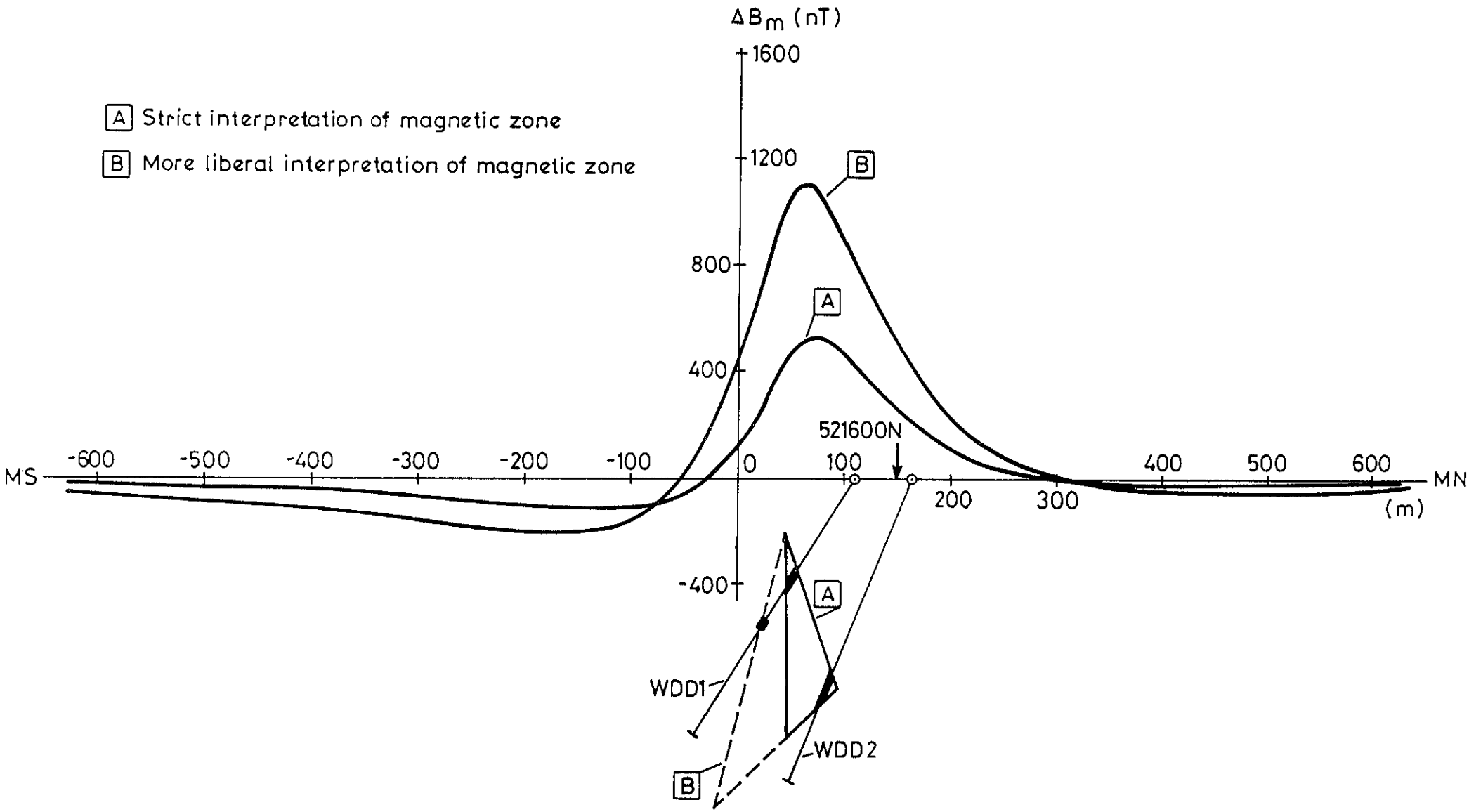

FIG. 5 SIMPLEST POLYGONAL MODELS OF INTERSECTED MAGNETIC ZONES

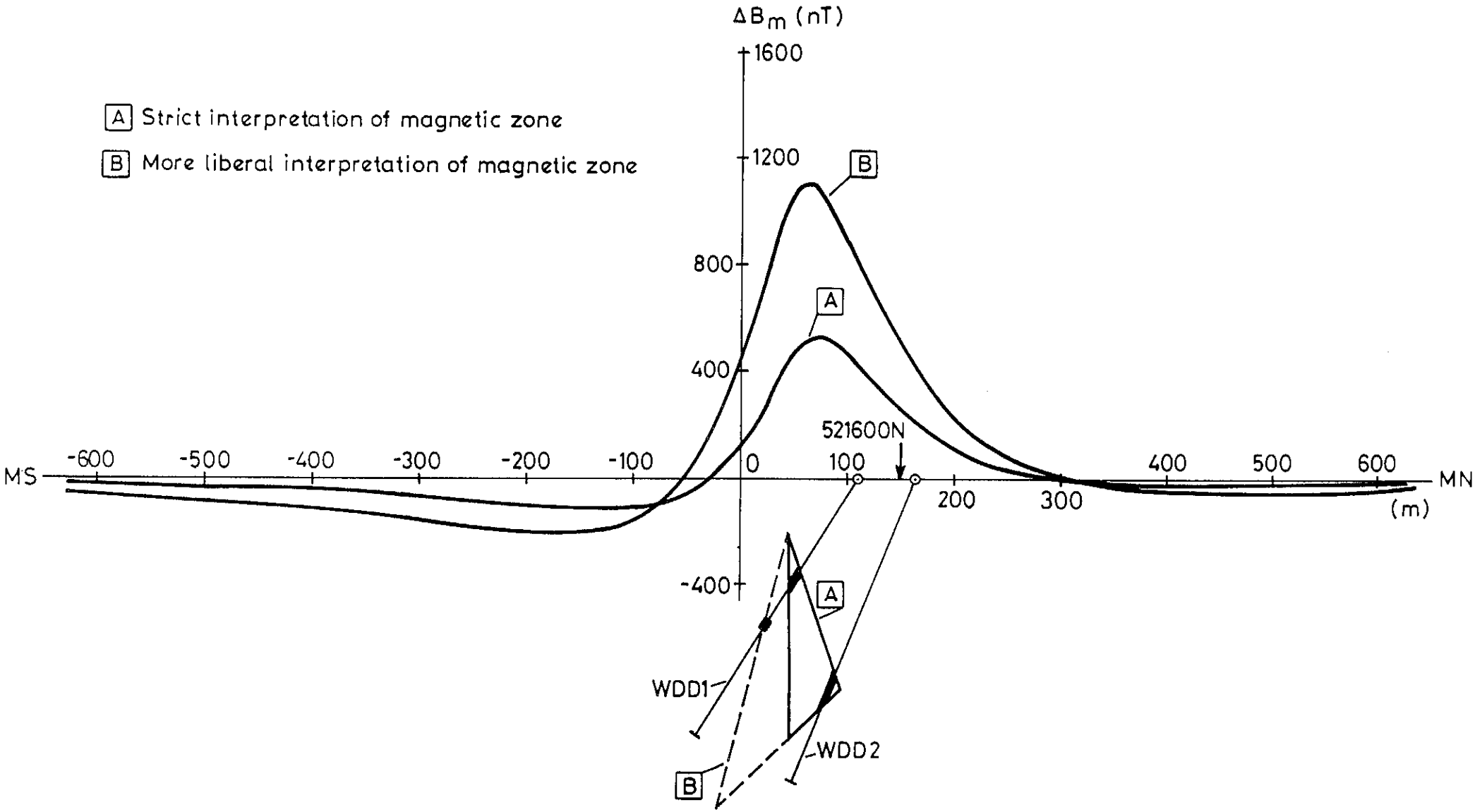

FIG. 5 SIMPLEST POLYGONAL MODELS OF INTERSECTED MAGNETIC ZONES

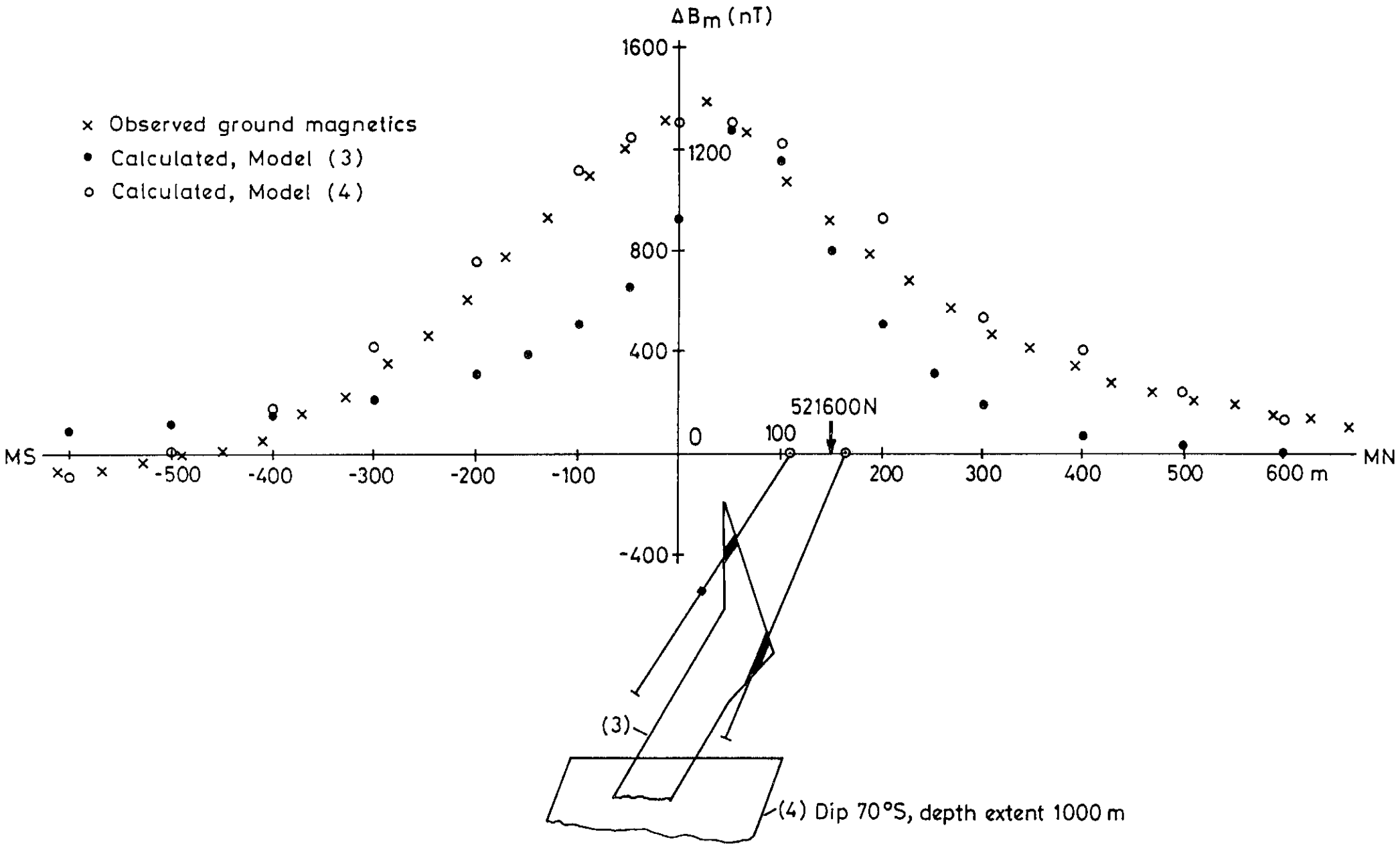

FIG. 6 ATTEMPTS TO EXPLAIN THE ANOMALY